Membrane Thinning Caused by Magainin 2[†]

Steve Ludtke, Ke He, and Huey Huang*

Physics Department, Rice University, Houston, Texas 77251-1892

Received August 11, 1995; Revised Manuscript Received October 16, 1995[⊗]

ABSTRACT: Magainin 2 is a 23-residue antibiotic peptide found in the skin of *Xeonpus laevis* (African clawed frog). It belongs to a broad class of α-helical peptides which interact directly with the lipid bilayer. Very little is presently known about the nature of this peptide/lipid interaction on the molecular level. We have performed a sequence of lamellar X-ray diffraction experiments to provide some insight into the nature of this interaction. We have found that, at concentrations below the critical concentration for lysis, the peptide causes the membrane thickness to decrease roughly in proportion to the peptide concentration. We further show that this thinning is consistent with a model where the peptide adsorbs within the headgroup region of the lipid bilayer at these concentrations. The energy cost of this thinning may also explain why the peptide inserts at high concentrations. We have already shown that a similar interaction exists for alamethicin interacting with diphytanoylphosphatidylcholine, and it should hold for a wide variety of peptide/lipid systems.

Magainin 2 is a 23-residue peptide which exhibits broad-spectrum antimicrobial activity (Zasloff, 1987): Gly-Ile-Gly-Lys-Phe-Leu-His-Ser-Ala-Lys-Lys-Phe-Gly-Lys-Ala-Phe-Val-Gly-Glu-Ile-Met-Asn-Ser. It is a member of a class of antimicrobial peptides found widely distributed in nature. Peptides in this class are from 18 to 50 residues long and form amphiphilic α-helices when associated with lipid bilayers (Boman et al., 1994). Examples include bombinin from amphibians (Gibson et al., 1991), alamethicin from fungi (Latorre & Alvarez, 1981), cecropins from moths (Steiner et al., 1981), melittin from bee venom (Habermann, 1972), and cecropin P1 from pig intestines (Lee et al., 1989). It has been shown that these peptides interact directly with the lipid bilayer rather than interacting with specific protein targets within the membrane (Bessalle et al., 1990; Wade et al., 1990). The primary function of all of these peptides is to rupture the cellular membrane of target cells. However, each peptide is active against a different subset of cell types. For example, magainin is a potent antimicrobial at relatively low concentrations, but it does not affect most normal eukaryotic cells unless the concentration is increased by roughly a factor of 100 (Cruciani et al., 1991; Zasloff, 1987). Melittin, on the other hand, is hemolytic and is an antibiotic even at low concentrations. The molecular mechanism for this selectivity is still unknown.

Recent studies have shown that below a (lipid-dependent) critical concentration magainin causes a permeability increase but does not lyse vesicles. Once the critical concentration has been reached, however, magainin rapidly causes widespread lysis (Matsuzaki et al., 1989, 1991). Solid-state NMR (Bechinger et al., 1991) and oriented circular dichroism have shown that at low concentrations magainin lies parallel to the membrane surface. However, at roughly the same critical concentration found in the leakage experiments, magainin begins to insert perpendicular to the membrane (Ludtke et al., 1994). At low concentrations, magainin has also been observed to form occasional ion channels (Duclohier et al., 1989; Cruciani et al., 1988, 1991). These data support a model wherein magainin adsorbs primarily on the membrane surface at low concentrations. When a transmembrane potential is applied, occasional oligomeric pores form, presumably due to the dipole moment of the α-helix. At high concentrations magainin inserts in bulk, causing large-scale membrane permeabilization or solubilization leading to cell lysis. The reason magainin goes from the surface state to the inserted state is still unknown. Understanding the nature of the interaction between the peptide and lipid on a molecular level is necessary for a complete understanding of magainin's cellular specificity.

To better understand the effect magainin has on the structure of the lipid bilayer, we have performed a series of X-ray diffraction studies of magainin in 3:1 POPC[1] (palmitoyloleoylphosphatidylcholine)/POPS (palmitoyloleoylphosphatidylserine) multilayers at various peptide concentrations and hydration states. The POPC/POPS system was chosen as a representative membrane with some charged headgroups. It has been shown that magainin interacts much more strongly with lipids with charged headgroups. However, pure charged membranes are much more fluid than their PC counterparts, making them much more difficult to work with in diffraction experiments. This binary lipid system is also favorable since it does not phase separate and it is in the L-α phase at room temperature. In this first study we have confined ourselves to concentrations below the critical concentration, that is, concentrations at which magainin is found lying primarily parallel to the membrane surface (Ludtke et al., 1994).

MATERIALS AND METHODS

Lipid was purchased from Avanti Polar Lipids Inc. (Alabaster, AL). Magainin 2 was donated by Magainin

[†] This work was supported in part by National Institutes of Health Grant AI34367 and Biophysics Training Grant GM08280, by Department of Energy Grant DE-FG03-93ER61565, and by the Robert A. Welch Foundation.

[⊗] Abstract published in *Advance ACS Abstracts,* December 1, 1995.

[1] Abbreviations: DPhPC, diphytanoylphosphatidylcholine; GC, gas chromatography; HTH, head to head distance; OCD, oriented circular dichroism; POPC, palmitoyloleoylphosphatidylcholine; POPS, palmitoyloleoylphosphatidylserine; TFE, trifluroethanol.

0006-2960/95/0434-16764$09.00/0

Pharmaceuticals Inc. Both lipid and peptide were used without further purification. Chloroform was purchased from EM Science and was certified 99.99% pure by GC (gas chromatography) with 1% ethanol. TFE was purchased from Sigma and was certified >99.95% pure by GC.

Sample Preparation. Our sample preparation method is based on our previous method for OCD using two substrates (Ludtke et al., 1994). The primary difference is that a single substrate is now used. While independently developed, this method is similar to that of Seul and Sammon (1990) and others. Samples were prepared on ~1 cm^2 glass microscope slides. Before use, each slide was cleaned abrasively and then soaked in a heated bath of sulfuric acid and chromic acid for 15−20 min, followed by repeated washing with distilled H_2O and ethanol. After a final ethanol wash the slide was allowed to air-dry. Lipid was deposited on the slide from a stock chloroform solution. Magainin was deposited from a stock TFE (trifluroethanol) solution. A typical magainin stock solution is ~1 mg/mL, and a typical lipid stock solution is 25 mg/mL. Typical samples used 1.5 mg of lipid and up to 0.1 mg of magainin. The mixture was then allowed to air-dry until all visible traces of the solvent were gone. Concentrations used in this experiment varied from pure lipid to a 65:1 molar ratio (lipid:peptide), although the method continues to produce good samples through at least 10:1. Some samples required the use of a larger volume of solvent than the slide could hold without spillage (with chloroform and TFE this limit is ~80 μL for a 1 cm^2 slide). In these cases, multiple depositions/evaporations were used. In some cases the slide was slowly tilted during the last stages of evaporation to obtain a more even coating. When the coating on the slide did not appear sufficiently uniform, the lipid/peptide mixture was redissolved in some combination of chloroform, TFE, and/or methanol. Finally, the sample is placed in a freeze-dryer to remove any remaining traces of solvent. The difficulty of preparing good samples using this method depends strongly on the specific lipid/peptide system in use.

The surface distribution of the final sample depends strongly on the solvents used during the evaporation process. The primary requirement is that the solvent system must have an appropriate surface tension and evaporation rate for the size of the substrate being used. For example, pure chloroform causes more sample to be deposited at the center of the substrate and tends to leave "rings" behind as it evaporates. Pure TFE, on the other hand, causes a very smooth deposition in the center of the slide, but most of the material aggregates along the edges of the substrate. Of course, chloroform evaporates much more rapidly than TFE, and what really matters is the surface tension near the end of the evaporation process. Additional difficulties arise when the lipid and peptide cannot be codissolved in one solvent. In this case, POPC is insoluble in TFE and magainin is insoluble in chloroform. Quite a bit of trial and error is required when working with a new lipid/peptide system, but once the method has been refined, new samples can be made quite rapidly and reproducibly. Typically three out of four samples are aligned and distributed evenly enough to provide good data.

Sample alignment was monitored by examining the crystalline mosaic as part of the X-ray diffraction experiment. This gives a direct measure of the alignment of the portion of the sample which is contributing to the Bragg peaks. The mosaic is typically a single strong peak surrounded by a small

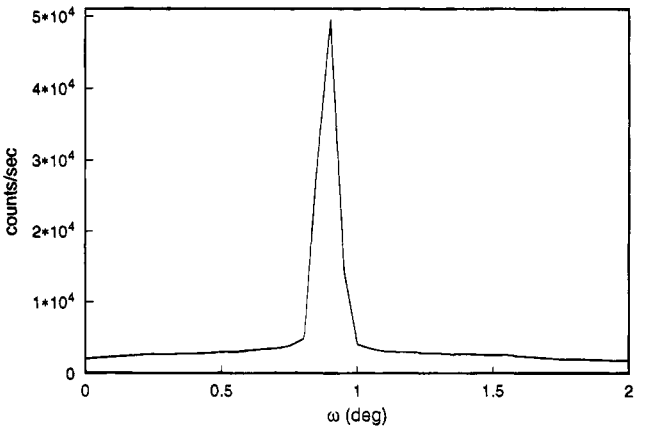

FIGURE 1: Typical crystalline mosaic of the first-order Bragg peak just before the $\omega-2\theta$ scan start. The humidity had not yet come to equilibrium at this point, causing a slight asymmetry in the peak. This peak is roughly as wide as the limiting resolution of our apparatus (~0.1°, due to detector slit size), implying extremely good alignment in the sample.

broad shoulder (Figure 1). The FWHM of the central maximum is ~0.1°, which corresponds to the limiting resolution of our experimental setup (due to slit settings). The broad shoulder is wider (>1°), but its small amplitude means it does not contribute significantly to the Bragg peaks. In general, this method of sample preparation provides as good an alignment or better than either of the two substrate methods used previously (Olah et al., 1991; Ludtke et al., 1994). In the previous methods, the sample was placed between two substrates and perturbed until the sample slowly reached alignment. There are several advantages to the new method using a single substrate: First, samples with two substrates take as long as 24 h to come to equilibrium when the relative humidity is changed, while single substrate samples come to equilibrium in just a few minutes. This reduces data collection time for a single sample from 2−3 weeks to 2−3 days. Second, the correction process becomes much simpler since absorbance by the second substrate is no longer a factor. Third, individual samples can be made in a single afternoon, while a large batch sample (used in one of the first two-substrate approaches) can take nearly a week to prepare. Finally, beryllium disks (which are quite expensive and difficult to keep in good shape) are no longer required. The main disadvantage of this method is nonuniformity in sample thickness. While it is possible to obtain samples that are fairly evenly distributed, the degree of uniformity is difficult to quantify.

Experimental Apparatus. Both relative humidity and temperature were controlled in the sample chamber during measurement. The temperature was held fixed with short-term stability better than ±0.1 °C and long-term (over 48 h) fluctuations of the order of ±0.4 °C. The humidity was controlled using a solid-state humidity probe (Phys-Chem Scientific Corp., New York) in a feedback loop with a temperature-controlled water bath. The impedance of the humidity probe is exponentially related to the relative humidity in the chamber with a very small temperature dependence. Variations in water temperature relative to sample temperature cause changes in the relative humidity felt by the sample. To ensure that the sample and probe were exposed to the same relative humidity, they were both attached to the same temperature-controlled surface. Both the sample and humidity probe were attached with silicone heat sink compound to ensure a good thermal contact. This

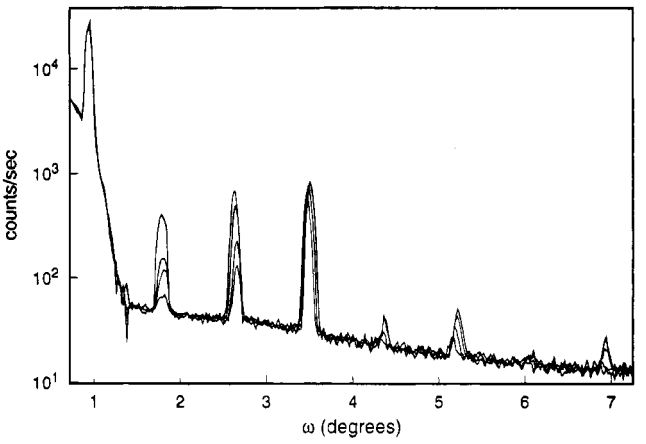

FIGURE 2: Typical diffraction spectra for pure 3:1 POPC/POPS. The four spectra were taken at different relative humidities. The only processing that has been done on these spectra is detector nonlinearity correction and compensation for the attenuator. The attenuator was turned off at 1.4°, hence the increased noise below that point. The broad shoulder that the first-order peak sits on is the trailing edge of the direct beam. Note the large change in the second- and third-order peaks as relative humidity changes.

system can hold the relative humidity constant to better than 1% with an absolute accuracy of ±2%. Samples are measured at ~27 °C. This is well above the T_m for both POPC (−2 °C) and POPS (14 °C). No phase separation (characterized by double peaks in the diffraction pattern) was observed for this system over the range of % RH and temperature used in this experiment.

X-rays were generated with a fixed anode, 1.5 kW fine focus X-ray tube operated at 25 mA and 40 kV. A graphite monochromator was used between the source and sample to obtain a nearly monochromatic Cu Kα beam. Slits were used before the detector and after the monochromator to limit beam size and divergence. The detector was a proportional counter with an integrated preamp/scaler. The scaler was set to exclude as much of the background as possible without losing an excessive number of diffracted photons. Data were collected using $\omega-2\theta$ scans. The intensity of the first-order Bragg peak is typically an order of magnitude larger than the second- to fourth-order peaks and causes the proportional counter to approach saturation. To prevent this without being forced to reduce the beam intensity, a 30× attenuator was used during data collection for the first-order peak. A typical lipid sample gives seven to nine clear Bragg orders (Figure 2).

Each sample was measured for ~4 h at each relative humidity setting. The first hour was excluded in each case since the relative humidity can take up to 45−50 min to stabilize at the new value. Integrated peak intensities for typical peaks in the first four Bragg orders are ~5 × 10^4 counts, giving a ~0.4% uncertainty in raw peak intensity. Uncertainties in the smaller peaks are larger, but they also contribute a correspondingly smaller amount to the final electron density profile.

Data Reduction. The data reduction process is similar to that used on earlier experiments (Wu et al., 1995; Olah et al., 1991). However, due to the change in sample geometry and the use of a different X-ray machine, a number of changes were made. As a test of the new method and correction routines, we reproduced our earlier published data for pure DPhPC (Wu et al., 1995) several times to within the margins of error.

The first step in data reduction is correction for detector nonlinearity. Given the detector dead time, τ, simple probabilistic analysis yields $m = re^{-r\tau}$, where m is measured counts per second and r is real counts per second. The dead time was measured, along with the attenuation coefficient of the attenuator, by measuring a range of beam intensities with the attenuator on and the same set of intensities with the attenuator off. The counts per second with the attenuator on was low enough that the dead time correction was small compared to the correction with the attenuator off. This curve was then fit to $c_{off} = Ac_{on}e^{-\tau Ac_{on}}$, where A is the attenuation of the attenuator, c is the measured number of counts with the detector on and off, and τ is the effective dead time. The fit gives $A = 26.5$ and $\tau = 2.6$ μs.

Next, the background was subtracted. The background curve was generated by removing all of the Bragg peaks from all of the data sets for a particular sample and then averaging the result together and interpolating over any remaining gaps. Given the range of humidities we use (70−98%), the gaps are quite small and only exist in the first and second Bragg orders.

A correction for sample size vs beam size was made. Given our experimental geometry, at small angles the projection of the beam onto the sample was larger than the sample itself. To correct for this, the direct beam profile is measured and then projected (mathematically) onto the surface of the sample. This yields the percent of the total beam intensity that is hitting the sample at any given angle.

In our previous experiments absorbance due to the Be substrate covering the sample was a significant effect, as was absorbance by the sample itself. With uncovered samples, thickness variations over the surface make accurate absorbance correction impossible. However, the effect is much smaller in this case. To estimate the effect ignoring absorbance will have on our results, we have performed the correction on several samples assuming a constant sample thickness. In this case, the relative amplitude corrections for first to fourth orders are approximately 8.5%, 3.5%, 1.5%, and 0.5%. Applying this correction to several data sets and comparing HTH distances with the uncorrected data give typical HTH distance corrections of 0.1−0.2 Å. The largest change we observed was 0.4 Å. As the data are reproducible to only ±0.5 Å, lack of absorbance correction should have a negligible effect on our results. To minimize any contributions absorbance may have on *relative* HTH distances, all samples in this experiment were made using the same amount of lipid.

Next we corrected for polarization and the Lorenz factor. In our geometry, the combined correction is simply $(1 + \cos^2 2\theta_B \cos^2 2\theta)/(\sin 2\theta)$, where θ_B is the Bragg angle of the monochromator.

Finally, the peaks are integrated to obtain amplitude and position. One final adjustment must be made to the peak positions before the data can be phased. The position of the sample in the beam was adjusted such that, at $\omega = 0$, the direct beam just skims the surface of the sample. Unfortunately, uncertainty in this adjustment can lead to a 1−2% inconsistency in repeat distance. Small errors in sample height are manifested as an approximately constant shift in all peak positions. This constant can be found by taking the y intercept of a plot of peak position vs peak order for all of the strong peaks in a data set. Then this is averaged over all scans for a particular sample. This constant is then subtracted from all of the peak positions.

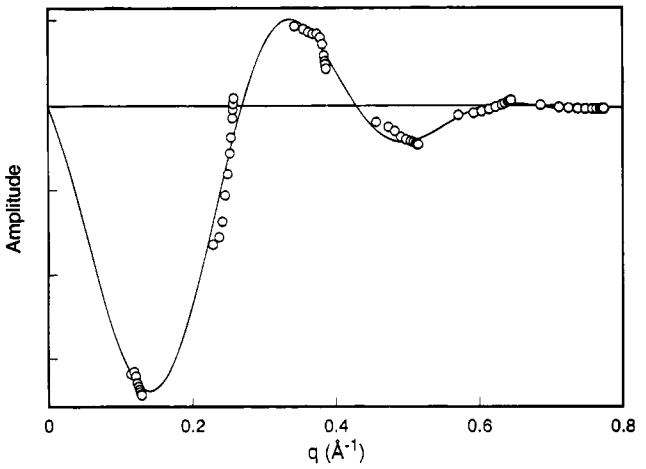

FIGURE 3: Representative phasing diagram for a sample with a 65:1 molar ratio. The solid line is the average of the fitting curves for all of the data sets. This line is not expected to fit the data exactly but is simply used as a guide for correctly phasing the data.

Phasing the peaks is accomplished using the well-known swelling method (Blaurock, 1971). Each diffraction pattern for a single sample must satisfy Blaurock's scaling relation: $\sum_n |F(2\pi n/D)| \propto D$, where n is Bragg order, F is the integrated peak amplitude, and D is the repeat distance. The constant of proportionality is chosen arbitrarily. Then, by plotting the peak positions and amplitudes of the same sample in various hydration states in q space and requiring that the data follow a smooth curve, the phases of the peaks can be determined unambiguously in most cases. In cases where there is insufficient variation to determine the phase unambiguously, a visual examination of the resulting electron density profile for both phases will usually show one to be a more reasonable choice (Olah et al., 1991; Torbet & Wilkins, 1976). A sample phasing diagram is shown in Figure 3.

With the phases known, the scattering amplitudes are then inverse Fourier transformed to obtain the scattering density ρ_{sc}, which is related to the true electron density ρ by $\rho = a\rho_{sc} + b$. The constants a and b arise from the fact that we did not measure absolute intensities and the zeroth order diffraction peak cannot be measured. However, since our results depend only on the position of the phosphate peaks, normalization of the electron densities is unnecessary and will be left in arbitrary units.

RESULTS

Representative electron density profiles are shown in Figure 4. Two sets of curves are shown: pure lipid and lipid with 60:1 magainin. We define the head to head (HTH) distance as the distance between the two phosphate peaks (peak position is defined as the point where $\partial\rho_{sc}/\partial z = 0$, where z is the coordinate normal to the bilayer). Note that this distance as well as the repeat distance is independent of electron density normalization. There are two effects evidenced in this figure. First, the addition of peptide clearly causes a significant reduction in HTH distance. A second effect is the reduction in HTH distance as hydration is increased.

These effects are shown more clearly in Figure 5 as a plot of HTH distance vs repeat distance for all four samples discussed in this paper. The repeat distance includes the water layer and is calculated directly from the spacing between the Bragg peaks in the raw data. The error bars in these curves are estimated from the reproducibility of the data. The uncertainty in HTH distance is primarily due to uncertainty in repeat distance. Even with all six to eight orders contributing to this value, the uncertainty in repeat distance is still ~0.5%. Other effects such as uneven sample distribution, uncertainty in P/L ratio, and temperature fluctuations also contribute slightly. The pure lipid curve

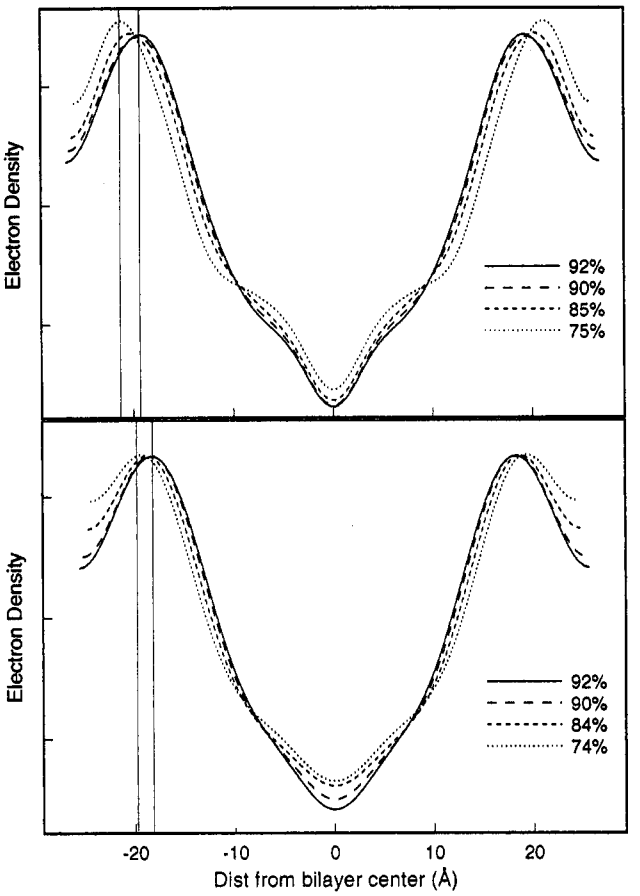

FIGURE 4: Electron density profile of the pure POPC/POPS sample (top) and the sample with a 65:1 lipid:magainin molar ratio (bottom) at various relative humidities. Note that the head to head distance *increases* as the relative humidity decreases. More importantly, the presence of magainin causes as substantial thinning.

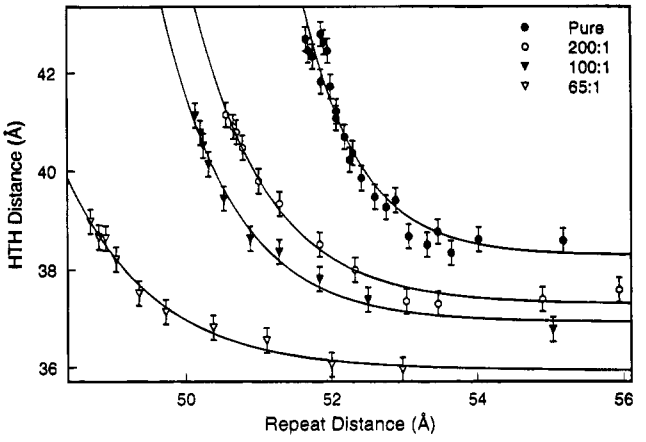

FIGURE 5: Variation of HTH distance with repeat spacing. This curve shows more clearly that as hydration increases for a given sample, the membrane actually becomes thinner. The solid lines are exponentials (plus a constant) and fit the curves quite nicely. Clearly the HTH distance approaches a limiting value as the samples approach full hydration. The addition of magainin does not have much effect on the shape of this curve, but it clearly causes the membrane to become thinner.

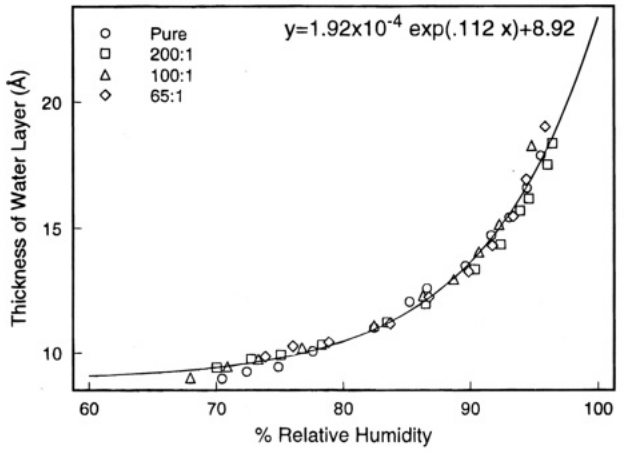

FIGURE 6: Water content versus relative humidity for all four samples. This curve was calculated by subtracting the HTH distance from the repeat distance for each sample at each relative humidity. This curve would be shifted slightly if water in the headgroup region and choline volume were compensated for. An exponential fits this curve quite accurately. Within the limits of uncertainty in our data, addition of magainin has no effect on this curve.

has been reproduced several times to well within the error bars. All four curves are fit very well by an exponential. Clearly, as hydration approaches 100%, the bilayer thickness approaches a limiting value. However, the most important effect to note is that magainin causes a significant decrease in membrane thickness roughly proportional to its concentration at all hydration levels.

Figure 6 shows thickness of the water layer vs relative humidity. The points in this plot were generated by subtracting the HTH distance from the repeat distance at each relative humidity setting for each sample. A portion of this distance is due to headgroup and peptide volume between the phosphates (in the water layer). Surprisingly, this figure shows that the thickness of the water layer appears to be independent of the peptide concentration. This implies that (at a constant relative humidity) the change in repeat distance caused when peptide is added to the system is almost entirely due to reduction of the membrane thickness, rather than changes in water layer thickness. If this holds generally, it will provide considerable freedom in future experiments, since the membrane repeat distance can be accurately measured even at very high peptide concentrations and hydrations (>98%) where there is an insufficient number of Bragg peaks to accurately calculate HTH distance. It is also interesting to note that the thickness of the water layer varies exponentially with relative humidity in this range. This curve implies that the repeat distance of the system becomes progressively less well defined as the hydration approaches 100%. This has been seen experimentally as the number of Bragg orders begins to decrease rapidly as 100% RH is approached. Carried to this limit, this implies that in excess water aligned multilayers will have a well-defined membrane thickness, but they will *not* have a well-defined repeat distance. We do not know if this situation would be different for MLVs (multilamellar vesicles), where the layers may be bound together by geometrical constraints.

DISCUSSION

The most interesting result in this experiment is the decrease in membrane thickness with the addition of magainin. This is very similar to the effect seen earlier in the alamethicin/DPhPC system (Wu et al., 1995). While surprising at first, this effect can be explained qualitatively using a simple geometric argument. When the peptide is adsorbed in the surface of the bilayer, it pushes the lipid headgroups aside. Since the total volume of the chains is constant, this causes the membrane to become thinner wherever a peptide molecule is adsorbed on the surface (Figure 7).

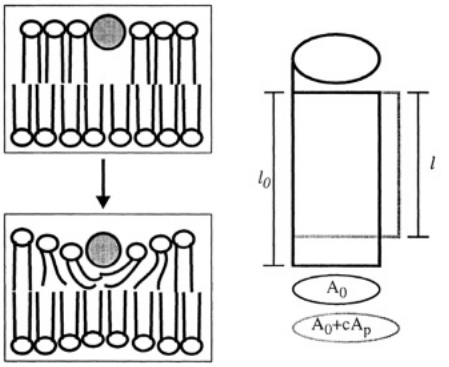

FIGURE 7: The adsorption of a peptide molecule in the headgroup region would force a gap in the chain region (upper left). For this gap to be filled, the membrane must become locally thinner (lower left). In our simplified model we approximate this as uniform thinning over the entire membrane. Each lipid molecule contributes $A_0(l_0 - l)$ toward filling the gap.

We can use this model to quantitatively predict the average membrane thinning caused by a given peptide concentration. In this model we ignore the shape of the depression caused by an individual peptide molecule and simply calculate the mean membrane thickness as if all lipid molecules were affected equally. The shape of the depression around the peptide will affect the width of the phosphate peak, but should have only a small effect on its position, so this approximation should be fairly accurate (S. J. Ludtke, K. He, and H. W. Huang, manuscript in preparation). We assume the peptide is adsorbed in the headgroup region of the bilayer without protruding significantly into the chain region. Requiring the chain volume to remain constant yields

$$l = \frac{A_0 l_0}{A} = \frac{A_0 l_0}{A_0 + cA_P} \tag{1}$$

A_0 and l_0 are the unperturbed surface area per lipid and chain length, A and l are the corresponding values with peptide present, c is the peptide concentration expressed as a molar fraction, and A_P is the surface area occupied by a peptide monomer.

Calculation of l_0 requires an estimate of the distance from the phosphate peak in the electron density profile to the beginning of the hydrocarbon chain. Using the results of a molecular dynamics simulation of 200 POPC molecules (Heller et al., 1993), we estimate this to be 4.5 ± 0.5 Å. In the high hydration limit, this gives l_0 = 14.6 Å. A_0 can be calculated using the HTH distance and a theoretical lipid volume. We calculated lipid volume by doing a Monte-Carlo integration of a molecular model of POPC using the van der Walls radius of each atom. Monte-Carlo integration was necessary due to the complexity of the structure and the large regions of overlap between atoms. This method yields a POPC volume of 1300 ± 20 Å^3. However, we really want the volume of the lipid between the two phosphate peaks. We can refine this number slightly using simulation results (Heller et al.,1993). Seventy-five percent of the volume of the choline group lies outside the region between the phosphates. This reduces our effective lipid volume by

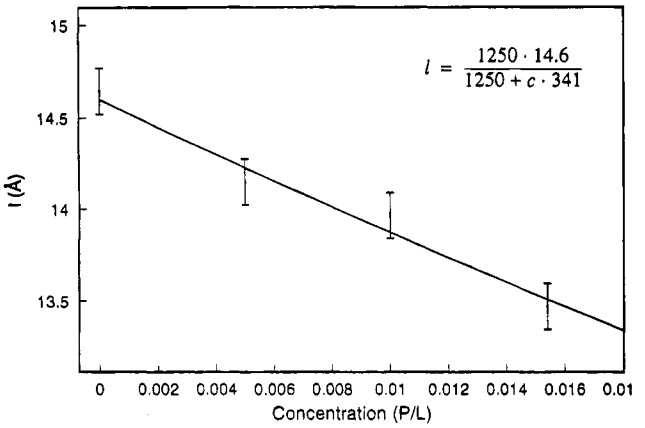

FIGURE 8: Effective lipid length vs peptide concentration. A fit of eq 1 to this curve gives 340 Å^2 for the surface area occupied by magainin.

~150 Å^3. However, we must also add in the volume occupied by water within the phosphate region. Water occupies ~100 Å^3 between the phosphate and the glycerol. These effects almost cancel each other out, giving an effective volume of 1250 Å^3. So, A_0 = 1250/(HTH distance/2) = 65 Å^2. This agrees well with other experimental results. In the L-α phase, Nagel and Wiener (1988) reported a value of 57.6−70.9 Å^2 for DPPC and Wiener and White (1992) reported a value of 60 Å^2 for DOPC.

Figure 8 shows a plot of l vs peptide concentration. With A_0 and l_0 determined, a fit of eq 1 to this curve yields A_P = 340 ± 30 Å^2. We can compare this to theoretical values for magainin. A Monte-Carlo integration of a molecular model of magainin gives a volume of 3500 Å^3. Magainin is a 23-residue α-helix, which makes it 34.5 Å long. If we assume that it is roughly cylindrical, this gives a theoretical value of A_P = 390 Å^2. If we make allowances for variations in side-chain size, this becomes ~300−450 Å^2 depending on orientation of the magainin about the helical axis, a very good match to our experimental value of 340 Å^2. In contrast, the cross-sectional area of an inserted magainin molecule would be ~100 Å^2. Clearly the data are consistent with this simple geometrical approximation where the peptide is adsorbed in the headgroup region.

CONCLUSIONS

We have shown conclusively that at low concentrations magainin causes the lipid bilayer to become thinner. This is very similar to the effect we observed when alamethicin was added to DPhPC multilayers, implying that this effect is probably common to the other peptides in this class as well. This behavior is consistent with a model where the peptide is adsorbed on the surface of the bilayer at low concentrations. This effect may also help to explain peptide insertion. As the peptide concentration increases, the membrane is forced to become thinner. Membrane deformation free energy increases quadratically with change of thickness (Huang, 1986), so the free energy increases roughly with the square of the concentration. So, peptide molecules should remain on the surface until the sum of the binding energy and the free energy of compression equals the energy of insertion. Experiments at higher concentrations and with other peptides are underway to give more information on this interaction.

We have also shown that, for this system, peptide concentration has little if any effect on the bilayer separation of the multilayer sample. At a given relative humidity, the thickness of the water layer was found to be constant to better than 1 Å independent of peptide concentration. This fact could be useful in further experiments where the repeat distance is readily measured, but the HTH distance cannot be easily obtained. Once a calibration curve has been measured for a given lipid system, the HTH distance could be calculated directly from the repeat distance. This will, of course, have to be verified in other lipid systems before this method can be used with any confidence.

ACKNOWLEDGMENT

We thank Dr. Michael Zasloff of Magainin Pharmaceuticals Inc. for his generous gift of magainin 2.

REFERENCES

Bechinger, B., Kim, Y., Chirlian, L. E., Gesell, J. , Neumann, J.-M., Montal, M., Tomich, J., Zasloff, M, & Opella, S. J. (1991) *J. Biomol. NMR 1*, 167−173.

Bessalle, R., Kapitkovsky, A., Gorea, A., Shalit, I., & Fridkin, M. (1990) *FEBS Lett. 274*, 151−155.

Blaurock, A. E. (1971) *J. Mol. Biol. 56*, 35−52.

Boman, H. G., Marsh, J., & Goode, J. A., Eds. (1994) *Antimicrobial Peptides, Ciba Foundation Symposium 186*, John Wiley & Sons, Chichester.

Cruciani, R. A., Stanley, E. F., Zasloff, M., Lewis, D. L., & Barker, J. L. (1988) *Biophys. J. 532*, 9 (Abstract).

Cruciani, R. A., Barker, J. L., Zasloff, M., Chen, H.-C., & Colamonici, O. (1991) *Proc. Natl. Acad. Sci. U.S.A. 88*, 3792−3796.

Duclohier, H., Molle, G., & Spach, G. (1989) *Biophys. J. 56*, 1017−1021.

Gibson, B. W., Tang, D., Mandrell, R., Kelly, M., & Spindel, E. R. (1991) *J. Biol. Chem. 266*, 23103−23111.

Habermann, E. (1972) *Science 177*, 314−322.

Heller, H., Schaefer, M., & Schulten, K. (1993) *J. Phys. Chem 97*, 8343−8360.

Huang, H. W. (1986) *Biophys. J. 50*, 1061−1070.

Jackson, M., Mantsch, H. H., & Spencer, J. H. (1992) *Biochemistry 31*, 7289−7293.

Latorre, R., & Alvarez, S. (1981) *Physiol. Rev. 61*, 77−150.

Lee, J. Y., Boman, A., Chuanxin, S., Andersson, M., Jornvall, H., Mutt, V., & Boman, H. G. (1989) *Proc. Natl. Acad. Sci. U.S.A. 86*, 9159−9162.

Ludtke, S. J., He, K., Wu, Y., & Huang, H. W. (1994) *Biochim. Biophys. Acta 1190*, 181−184.

Matsuzaki, K., Harada, M., Handa, T., Funakoshi, S., Fujii, N., Yajima, H., & Miyajima, K (1989) *Biochim. Biophys. Acta 981*, 130−134.

Matsuzaki, K., Harada, M., Funakoshi, S., Fujii, N., & Miyajima, K. (1991) *Biochim. Biophys. Acta 1063*, 162−170.

Nagel, J. F., & Wiener, M. C. (1988) *Biochim. Biophys. Acta 942*, 1.

Olah, G. A., Huang, H. W., Liu, W., & Wu, Y. (1991) *J. Mol. Biol. 218*, 847−858.

Steiner, H., Hultmark, D., Engstrom, A., Bennich, H., & Boman, H. G. (1981) *Nature 292*, 246−248.

Torbet, J., & Wilkins, M. H. F. (1976) *J. Theor. Biol. 62*, 447−458.

Wade, D., Boman, A., Wåhlin, B., Drain, C. M., Andreu, D., Boman, H. G., & Merrifield, R. B. (1990) *Proc. Natl. Acad. Sci. U.S.A. 87*, 4761−4765.

Wiener, M. C., & White, S. H. (1992) *Biophys. J. 61*, 428.

Wu, Y., He, K., Ludtke, S. J., & Huang, H. W. (1995) *Biophys. J. 68*, 2361−2369.

Zasloff, M. (1987) *Proc. Natl. Acad. Sci. U.S.A. 84*, 5449−5453.

BI9518860